ELSEVIER

Materials Science and Engineering A192/193 (1995) 186-194

MATERIALS SCIENCE & ENGINEERING A

Nickel aluminide containing refractory-metal dispersoids: 1: Synthesis by reactive mechanical alloying

T. Takahashi*, D.C. Dunand

Department of Materials Science and Engineering, Massachusetts Institute of Technology, Cambridge, MA 02139, USA

Abstract

Nickel and aluminum powders were mechanically alloyed with 10 or 30 vol.% refractory metal powders (molybdenum or tungsten) for times up to 50 h. Intermetallic synthesis takes place after 10-20 h alloying, with concomitant dispersion of the inert refractory metal phase, resulting in an NiAl matrix containing fine refractory dispersoids. The reactive synthesis step is direct, without intermediate intermetallic products. In a separate processing route, the compound NiMo was first synthesized by hydrogen reduction of nickel oxide and molybdenum oxide. Subsequent reactive mechanical alloying of NiMo powders with metallic nickel and aluminum powders yielded the same phases as the direct route from elemental powders. However, the dispersion step is more efficient with brittle NiMo than with ductile molybdenum, leading to a finer molybdenum dispersion size in the reacted powders. All mechanically alloyed powders are stable on exposure for 1 h at 1000 °C in a reducing atmosphere, but oxidize rapidly in air between 425 °C and 1000 °C.

Keywords: Nickel; Aluminium; Alloys; Refractory metals

1. Introduction

The stoichiometric intermetallic phase NiAl forms a simple eutectic in the pseudo-binary phase diagrams with many transition metals: vanadium [1-3], chromium [2,4-6], molybdenum [7-10], tungsten [2,4,11] and rhenium [12-14]. Of these metals, molybdenum and tungsten are of particular interest owing to their high melting points, high specific strengths at room and elevated temperature, and high eutectic temperatures with NiAl. The NiAl-Mo eutectic takes place at a temperature of 1600 °C and a composition of 10 at.% Mo (20 wt.% Mo) [10]; the NiAl-W eutectic temperature is 1600 °C as well, at a composition of 1.4 at.% W (6.1 wt.% W) [2,4,11]. However, the casting route only allows limited control of the volume fraction, size and morphology of the refractory second phase. While directional solidification can result in *in situ* refractory fibers in an NiAl matrix [15,16], it is difficult to form a dispersion of fine refractory particles since coarsening is expected to take place near the eutectic temperature. Composites with large refractory particles (typically above 1 μm) can be fabricated by hot-compaction of mixed powders of prealloyed NiAl and refractory metals [17]. Owing to the large interparticle distance, these composites however exhibit negligible dispersion strengthening and, since the particles are equiaxed, only modest composite strengthening is expected [18].

Fine homogenous mixtures of immiscible phases can be achieved by mechanical alloying as a result of the repetitive welding and fracturing of the powders during the process [19,20]. Thus, if a powder mixture of prealloyed NiAl and insoluble transition metal is milled, a fine dispersion of the minority phase is expected to form within the majority phase. Because of the difficulty of fabricating powders of the high-melting point NiAl, synthesis of the aluminide during the mechanical alloying step from elemental powders has been recently developed [21-25]:

$$\mathrm{Ni} + \mathrm{Al} = \mathrm{NiAl} \quad (1)$$

Additions to the elemental powders of further reactive or non-reactive species during mechanical alloying can also result in NiAl containing a dispersion of nitrides [26-29], oxides [30-33] or metals and compounds [34].

*Present address: Department of Inorganic Materials, Hyogo Prefectural Institute of Industrial Research, Kobe 654, Japan.

SSDI 0921-5093(94)03234-3

In the present paper (part 1), we describe the synthesis of NiAl powders containing 10 and 30 vol.% submicrometer molybdenum or tungsten dispersoids, formed by reactive mechanical alloying of elemental or intermetallic powders. In a companion paper (part 2) [35], we examine the microstructure and dispersion-strengthening of bulk samples prepared by hot isostatic pressing of these mechanically alloyed powders.

2. Experimental procedures

Five different alloy powders were synthesized with overall composition NiAl, NiAl–10 vol.% Mo, NiAl–30 vol.% Mo, NiAl–10 vol.% W and NiAl–30 vol.% W, referred to in the following as NiAl, NiAl–10 Mo, NiAl–30 Mo, NiAl–10 W and NiAl–30 W respectively. The powders were mechanically alloyed under static argon cover gas at room temtemperature. Batches of 30 g powders with 0.3 ml methanol were processed in a vibratory mill (Spex mixer/miller 8000) in a stainless steel vial with five hardened chromium-steel balls 8.36 g each. Two processing routes were explored, referred to in the following as the metal route and the intermetallic route respectively.

In the metal route, the NiAl–Mo and NiAl–W dispersions are synthesized directly from elemental powders:

$$a\text{Ni} + a\text{Al} + b\text{Mo} = a\text{NiAl} + b\text{Mo} \quad (2a)$$

$$a\text{Ni} + a\text{Al} + b\text{W} = a\text{NiAl} + b\text{W} \quad (2b)$$

The powders used were 99.9% nickel from Johnson Matthey with sizes between 74 μm and 149 μm, 99.8% aluminum powder from Johnson Matthey with sizes between 44 μm and 420 μm, 99.95% tungsten from Johnson Matthey with an average size of 12 μm and 99.95% molybdenum from Climax Specialty Metals with an average size of 5 μm. Scanning electron microscopy (SEM) showed that the powders were equiaxed with smooth surfaces.

In the intermetallic route, the oxides of nickel and refractory metal are mixed in the vibratory mill for about 2 h, loaded in an alumina crucible and reduced at 1000 °C for 2 h under flowing pure hydrogen or an Ar–4% H_2 mixture, to synthesize stoichiometric mixtures of finely dispersed metals:

$$\text{NiO} + \text{MoO}_3 + 4\text{H}_2 = \text{Ni} + \text{Mo} + 4\text{H}_2\text{O} \quad (3a)$$

$$\text{NiO} + \text{WO}_3 + 4\text{H}_2 = \text{Ni} + \text{W} + 4\text{H}_2\text{O} \quad (3b)$$

On diffusion, the intermetallic phases MoNi and NiW respectively can then be formed. Powders from Johnson Matthey were used: 99% nickel oxide less than 44 μm in size, 99.95% molybdenum oxide and 99.8% tungsten oxide.

In a second step, the intermetallic intermediate phases are mechanically alloyed with aluminum and nickel to form NiAl–Mo and NiAl–W respectively:

$$(a-b)\text{Ni} + a\text{Al} + b\text{MoNi} = a\text{NiAl} + b\text{Mo} \quad (4a)$$

$$(a-b)\text{Ni} + a\text{Al} + b\text{NiW} = a\text{NiAl} + b\text{W} \quad (4b)$$

Table 1 gives the chemical composition of the initial powders for all samples. At fixed time intervals during the mechanical alloying process, powder samples were extracted, mounted in epoxy, characterized by X-ray diffraction with Cu Kα radiation and a graphite monochromator, and polished by standard procedures for metallographic observation.

Loose mechanically alloyed powders were also loaded in an alumina crucible and heat treated at varying temperatures for 1 h under vacuum or an Ar–4% H_2 atmosphere, before being subjected to X-ray diffraction.

Thermogravimetry experiments were performed with about 50 mg loose powder which had been mechanically alloyed for 20 h and hydrogen annealed for 1 h at 1000 °C. The mass gain was measured under continuous heating conditions at a rate of 600 K h^{-1} with air flowing at 3 l h^{-1}.

3. Results

Fig. 1 shows the X-ray spectra of the refractory-free, stoichiometric nickel–aluminum mixtures. Both peaks corresponding to Ni (200) and Al (111) disappear between 5 h and 10 h milling, while the main NiAl (110) peak, which partially overlaps the Ni (111) and Al (200) peaks, appears in the same time period.

Figs. 2(a) and 2(b) show the X-ray spectra for NiAl–10Mo and NiAl–30Mo respectively, processed by the metal route (Eq. (2a)). Between 10 h and 20 h

Table 1
Chemical composition of initial powders used in mechanical alloying

Sample	Ni (wt.%)	Al (wt.%)	Refractory (wt.%)	Intermetallic (wt.%)
NiAl	68.6	31.4	—	—
NiAl–10Mo	57.5	26.5	16.0Mo	—
NiAl–10Mo (I)	47.7	26.5	—	25.8MoNi
NiAl–30Mo	39.5	18.1	42.4Mo	—
NiAl–30Mo (I)	13.5	18.1	—	68.4MoNi
NiAl–10W	50.4	23.1	26.5W	—
NiAl–10W (I)	41.9	23.1	—	35.0NiW
NiAl–30W	28.7	13.2	58.2W	—
NiAl–30W (I)	10.1	13.2	—	76.7NiW

milling, the Ni (200) and Al (111) peaks disappear while the NiAl (110) peak appears, indicating synthesis of NiAl. The Mo (110) peak is present at all times and broadens with increasing milling time. Mo_2C is formed by reaction of molybdenum with the small amounts of methanol added to the powders as anti-caking agent.

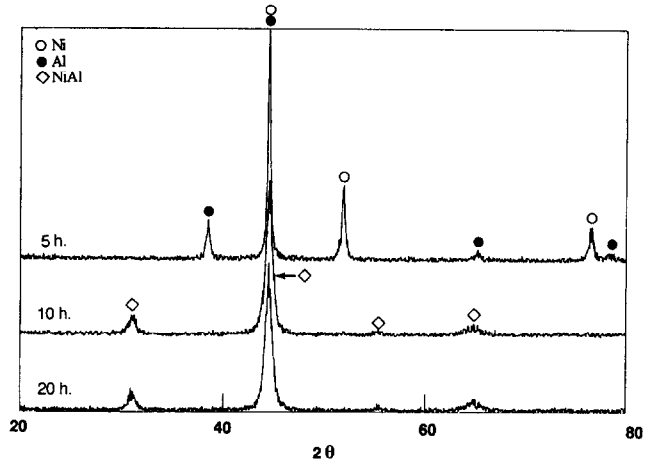

Fig. 1. X-ray spectra as a function of alloying time for NiAl synthesized from metallic powders (Eq. (1)).

In Figs. 3(a) and 3(b), the X-ray spectra for NiAl–10W and NiAl–30W are given for the metallic route (Eq. (2b)); as for the NiAl–Mo system, the peaks corresponding to the refractory metal are present at all times, indicating no significant formation of intermediate intermetallic compound. W_2C forms by reaction between tungsten and the small amounts of methanol. However, NiAl synthesis seems to be more rapid, as the main Ni and Al peaks disappear between 5 h and 10 h alloying.

Hydrogen reduction of the mixed oxides of molybdenum and nickel leads to a product with an X-ray spectrum exhibiting none of the peaks for the elemental powders (Fig. 4). SEM observation shows that the product is porous (Fig. 5), with cell wall thickness less than 1 μm. However, X-ray analysis of the reduction products of the mixed oxides of tungsten and nickel with overall composition of $Ni_{50}W_{50}$ indicates the presence of a large amount of metallic tungsten, together with one or more intermetallic phase, presum-

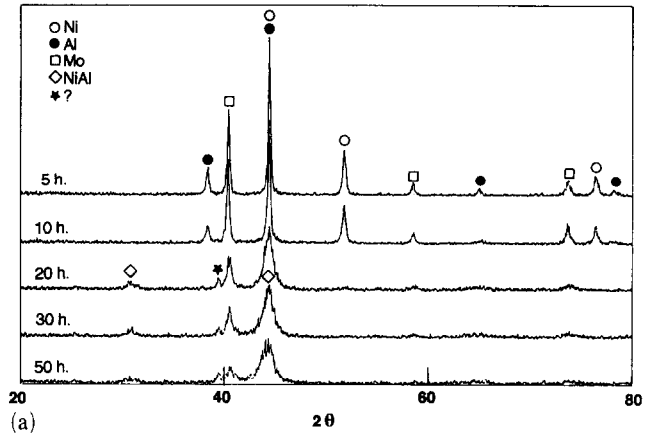

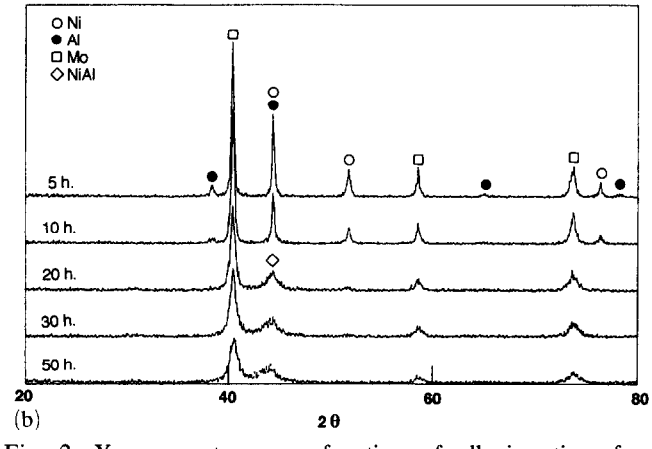

Fig. 2. X-ray spectra as a function of alloying time for NiAl–10Mo (a) and NiAl–30Mo (b) synthesized by the metal route (Eq. (2a)). Peaks marked with a star correspond to Mo_2C.

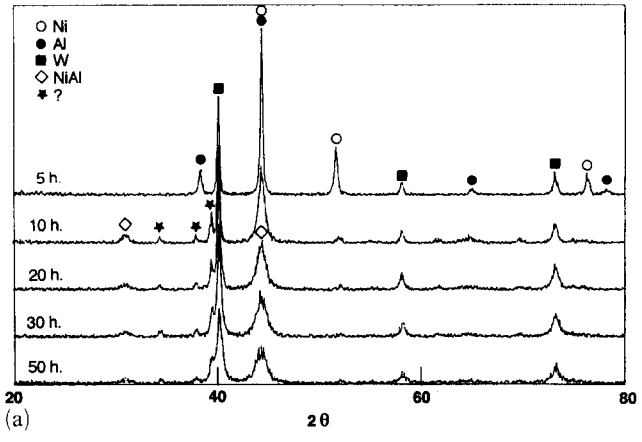

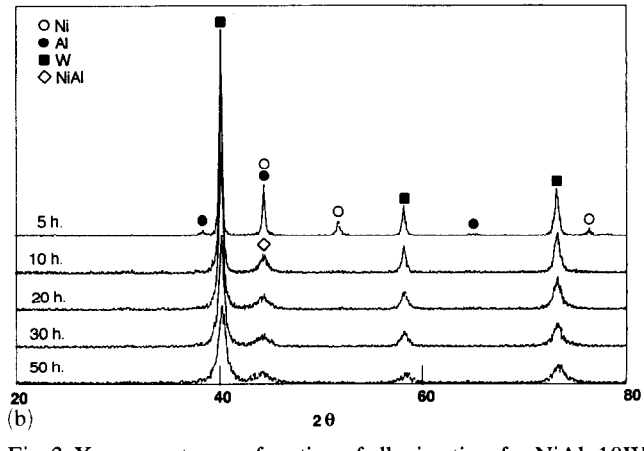

Fig. 3. X-ray spectra as a function of alloying time for NiAl–10W (a) and NiAl–30W (b) synthesized by the metal route (EQ. (2b)). Peaks marked with a star correspond to W_2C.

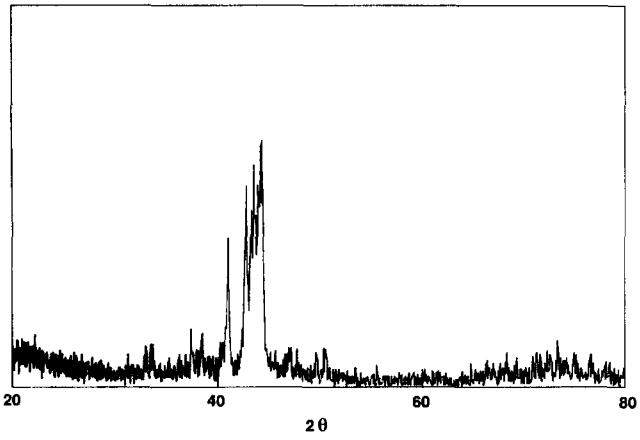

Fig. 4. X-ray spectrum of MoNi synthesized by oxide reduction at 1000 °C in an Ar–4%H_2 mixture (Eq. (3a)).

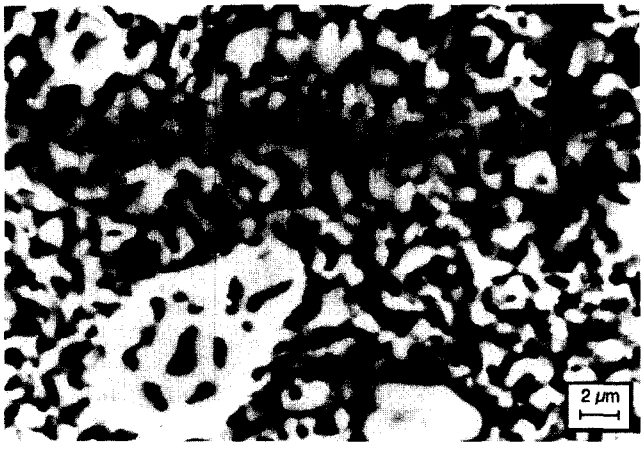

Fig. 5. SEM image of MoNi reduced at 1000 °C from oxide powders.

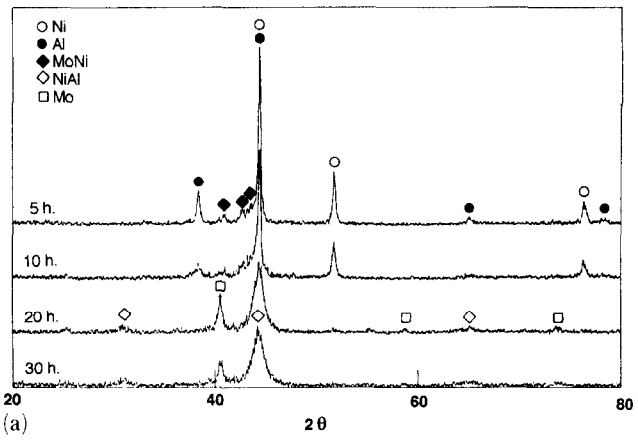

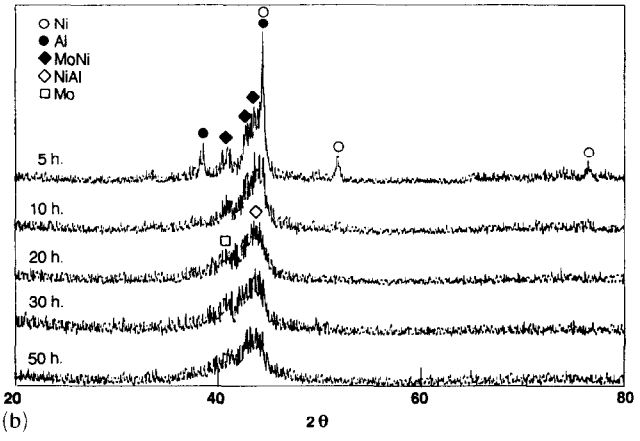

Fig. 6. X-ray spectra as a function of alloying time for NiAl–10Mo (a) and NiAl–30Mo (b) synthesized by the intermetallic route (Eq. (4a)).

ably NiW. While further synthesis by mechanical alloying of NiAl–10W and NiAl–30W was completed with success with this metallic–intermetallic mixture according to Eq. (4b), the results are not reported in the following since the fraction and composition of the phases of the $Ni_{50}W_{50}$ mixture were unknown.

Figs. 6(a) and 6(b) show the X-ray spectra of NiAl–10Mo and NiAl–30Mo respectively, processed by the intermetallic route (Eq. (4a)) from the MoNi powders produced by hydrogen reduction. The Ni (200) and Al (111) peaks disappear between 10 h and 20 h for NiAl–10Mo and between 5 h and 10 h for NiAl–30Mo. For NiAl–10Mo, the series of peaks corresponding to MoNi (Fig. 4) disappears while the (110) NiAl peak and (110) Mo peak appear between 10 h and 20 h, corresponding to the reaction given in Eq. (4a). While the large broadening of peaks in Fig. 6(b) does not allow a clear interpretation, the spectrum evolution for NiAl–30Mo seems to be similar to that of NiAl–10Mo (Fig. 6(a)).

Figs. 7(a) and 7(b) show the microstructure of a polished powder particle from the NiAl–10Mo powders processed by the metal and intermetallic routes respectively, after 10 h milling, i.e. before significant NiAl synthesis. The particle consists of an unreacted mixture of the initial phases: the higher the atomic number of the phase, the lighter the contrast appears on the micrographs. Powder particles from the same samples after 30 h alloying exhibit a uniformly reacted matrix containing fine molybdenum dispersoids. Figs. 8(a) and 8(b) show the evolution of refractory particle size as a function of milling time for NiAl–30W processed by the metal route; the dispersoids within the powder particles become smaller and more equiaxed as the alloying time increases.

Fig. 9 shows the X-ray spectra of NiAl–10Mo mechanically alloyed for 50 h by both routes (Eq. (2a) or Eq. (4a)) after a 1 h anneal at 1000 °C under an Ar–4%H_2 atmosphere. Similar spectra were recorded for NiAl–30Mo processed identically. In all cases, the peaks belonging to NiAl and the refractory metal are sharp, and no peaks corresponding to aluminum or

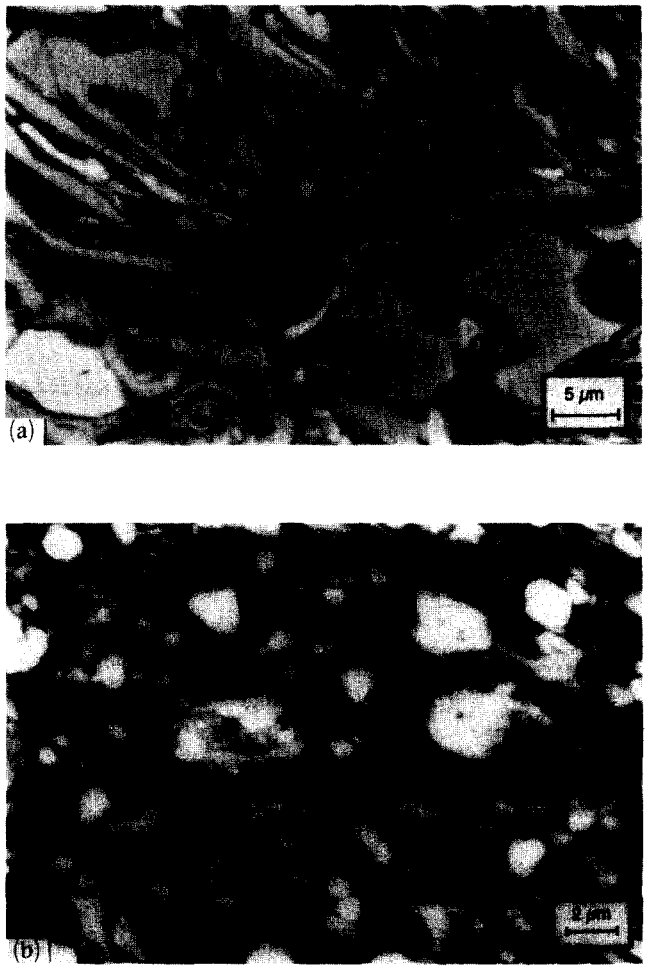

Fig. 7. SEM images of powder particles from NiAl–10Mo after 10 h mechanical alloying (a) by the metal route and (b) by the intermetallic route.

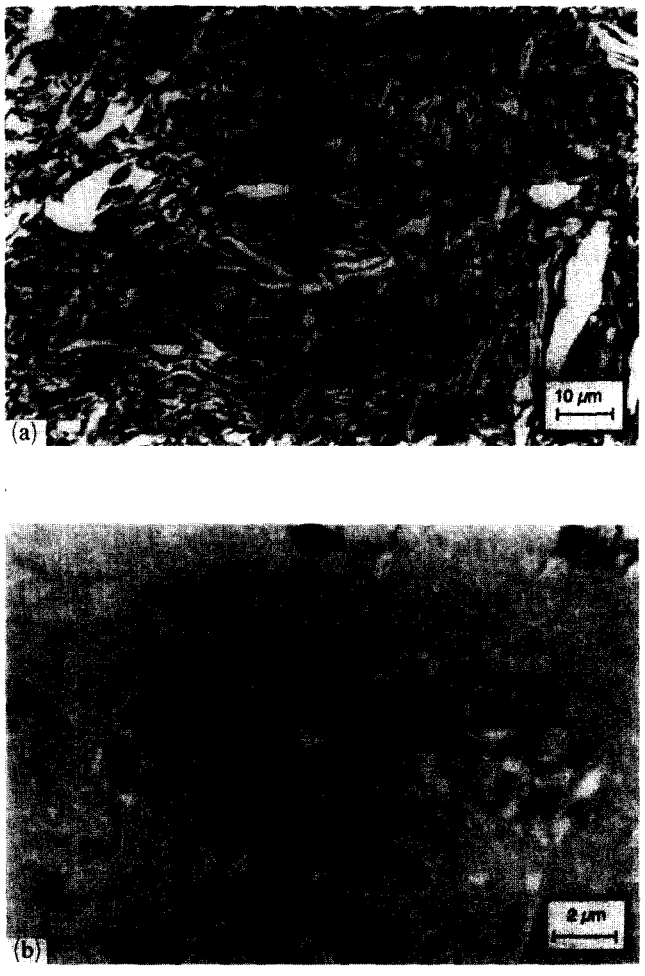

Fig. 8. SEM images of powder particles from sample NiAl–30W after (a) 10 h and (b) 30 h mechanical alloying by the metal route.

nickel are present. Similar results were found for NiAl–10Mo powders alloyed for 20 h after a 1 h anneal at 1000 °C under vacuum.

Fig. 10 gives the X-ray spectra of NiAl–10W powders processed by the metal route (Eq. (2b)) for 50 h and annealed in Ar-4%H_2 for 1 h at temperatures between 600 and 1000 °C. Annealing results in a sharpening of the peaks which become narrower with increasing heat treatment temperature. Similar results were found for NiAl–30W powders after the same heat treatment schedules.

Fig. 11 shows thermogravimetric curves for the mechanically alloyed powders with and without 10 vol.% refractory phase. All refractory-containing samples exhibit larger mass gains than the pure NiAl sample. A steep mass increase is observed for the molybdenum-containing samples near 800 °C, corresponding to the melting point of MoO_3.

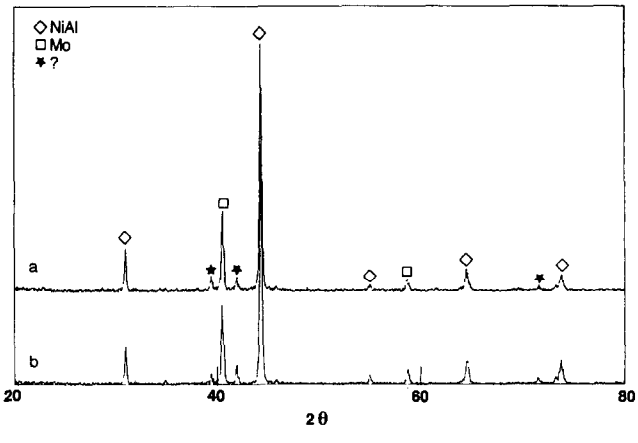

Fig. 9. X-ray spectra of NiAl–10Mo synthesized by the metal route (a) and the intermetallic route (b) (50 h alloying time) and annealed for 1 h at 1000 °C under Ar–4%H_2. Peaks marked with a star correspond to Mo_2C.

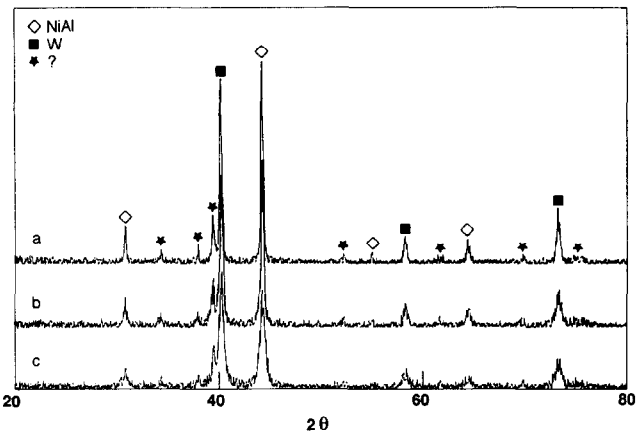

Fig. 10. X-ray spectra of NiAl–10W synthesized by the metal route (50 h alloying time) and annealed for 1 h at (a) 1000 °C, (b) 800 °C, (c) 600 °C under Ar–4%H_2. Peaks marked with a star correspond to W_2C.

4. Discussion

4.1. Powder synthesis

As shown in Fig. 1, synthesis of refractory-free NiAl from the metallic reactants occurs directly according to Eq. (1), without measurable formation of the intermediate intermetallics observed in nickel–aluminum diffusion couple experiments [36,37]. The X-ray peaks broaden with increasing milling time, indicating grain refinement and cold work. The above observations are in agreement with earlier studies on reactive mechanical alloying of NiAl [23,25,38–40]. NiAl synthesis is not markedly affected by the presence of metallic molybdenum or tungsten (Figs. 1–3); the time for NiAl formation is similar and no binary or ternary refractory-containing phases are detected in the X-ray diffraction patterns, with the exception of refractory carbides formed by reaction between the refractory metals and methanol. Slight deviations from stoichiometry may have been responsible for the formation of some of the equilibrium phases present in the Ni–Al–Mo system [2,4,10] and Ni–Al–W system [11] respectively. The formation of oxides during mechanical alloying due to oxygen contamination from the methanol is also possible. Contamination of the powder by the vessel and grinding balls is unlikely, since wet-chemical analysis of NiAl–30Mo mechanically alloyed for 50 h indicates only small levels of foreign elements: 0.16 wt.% Fe for the metal route and 0.11 wt.% Fe and 0.033 wt.% Cr for the intermetallic route.

Since MoNi melts incongruently at 1362 °C, it cannot be synthesized easily by solidification; a melt with overall composition MoNi forms primary molybdenum between 1680 °C and 1362 °C, prior to solidification at 1309 °C of an eutectic consisting of MoNi and a solid solution of molybdenum in nickel [41], as shown in Fig. 12 for an arc-melted sample with overall composition $Mo_{50}Ni_{50}$. Since the X-ray spectrum of the hydrogen-reduced oxides of molybdenum and nickel shows no peaks corresponding to the oxides or the metals (Fig. 4), it can be concluded that the oxides were reduced and the intermetallic MoNi was formed by diffusion between the two metal phases. Since both NiO and MoO_3 are unstable in the presence of pure hydrogen [42], Eq. (3a) is indeed expected to proceed. Some loss of molybdenum may have occurred, since MoO_3 melts at 795 °C and has a significant vapor pressure at 1000 °C [42]. The synthesis of NiW by hydrogen reduction was not successful, since significant amounts of metallic tungsten were detected in the hydrogen-reduced powder. A possible explanation is that, owing to the very high melting point of tungsten, diffusion was too slow to form the equilibrium intermetallic phase from the mixture of metal phases resulting from the hydrogen reduction. Because intermetallic MoNi is expected to be more brittle than molybdenum, and because a prealloying step had been carried out (Eq. (3a)), the reactive mechanical alloying kinetics for the intermetallic route (Eq. (4a)) were expected to be faster than for the metal route (Eq. 2(a)). Comparison of Figs. 2 and 6 however indicates no significant difference for the kinetics of NiAl formation between the two routes; in both cases, the peaks corresponding to the metallic reactants disappear, and the NiAl peaks appear between 10 h and 20 h milling. As with the metallic route, no measurable intermediate species are present in Fig. 6, indicating that Eq. (4a) proceeds directly. Annealing at 1000 °C yields an X-ray spectrum (Fig. 9(b)) which is virtually identical with that from the annealed powders synthesized by the metal route (Fig. 9(a)).

Figs. 7(a) and 7(b) show however that the morphology of the powders after 10 h mechanical alloying (i.e. before large-scale NiAl synthesis) varies according to the processing route. With the metal route (Fig. 7(a)), the powder particles consist of lamellae of the three elemental metals, as expected for an all-ductile system. The molybdenum phase (brightest phase in Fig. 7(a)) shows a wide distribution of size, from less than 1 μm to about 5 μm. With the intermetallic route (Fig. 7(b)), the powder microstructure consists of a lamellar matrix of elemental nickel and aluminum containing equiaxed dispersoids with high atomic number, most probably MoNi since NiAl synthesis has not taken place (Fig. 6). The size of the MoNi dispersoids in Fig. 7(b) is significantly smaller than that of molybdenum in Fig. 7(a), as expected since the MoNi intermetallic reactant has a

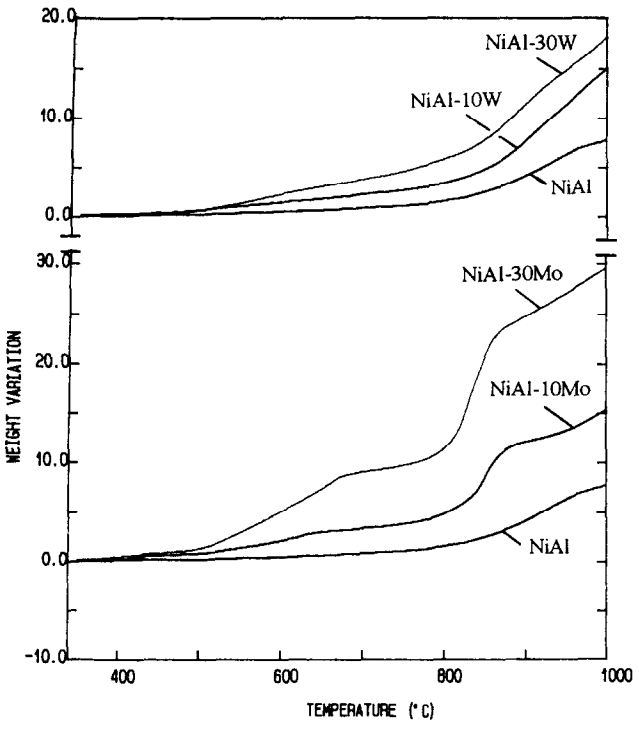

Fig. 11. Thermogravimetric curves for mechanically alloyed (20 h) hydrogen-annealed powders.

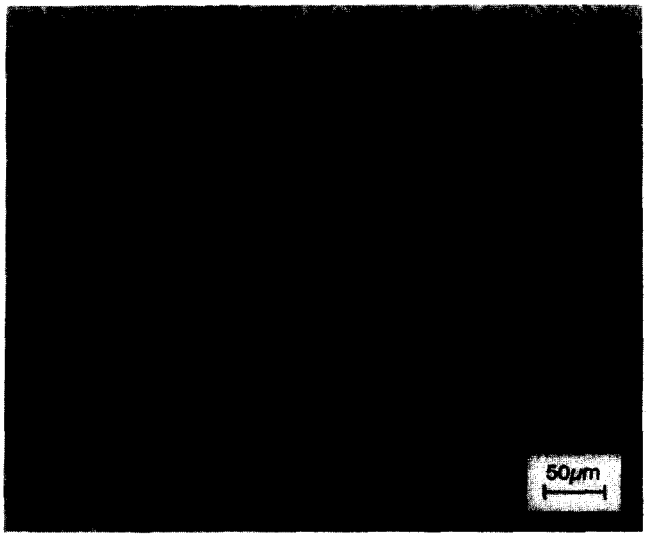

Fig. 12. Arc-melted alloy with overall composition 50 at.% Ni and 50 at.% Mo. Primary molybdenum is formed, followed by eutectic solidification of Ni–MoNi.

finer structure (Fig. 5) than the initial molybdenum particles. Furthermore, the MoNi dispersoids are equiaxed after 10 h milling (Fig. 7(b)), unlike the molybdenum phase (Fig. 7(a)) which is elongated, as expected from the brittle nature of MoNi and the ductile nature of molybdenum respectively. We conclude that the dispersion of molybdenum is more efficient by the intermetallic route, as a result of the small size and low ductility of MoNi; furthermore the transfer reaction (Eq. 4(a)) may also contribute to a finer dispersion.

Figs. 8(a) and 8(b) for NiAl–30W after 10 h and 30 h mechanical alloying respectively, illustrate the refinement of the dispersoids with increasing alloying time. After 10 h milling, the tungsten size distribution is similar to that of molybdenum in Fig. 7(a); the flattened morphology indicates that tungsten deforms plastically on impact during alloying. After 30 h milling, the tungsten particles are much smaller (Fig. 7(b)) and, while the size of the particles is below 0.5 μm, some particles as large 2 μm are still visible, indicating that the refinement is progressive. We note that once the brittle NiAl matrix replaces the ductile nickel–aluminum mixture, faster refinement of the refractory metal may occur, since fracture of the NiAl is expected to take place more frequently.

4.2. *Powder stability at elevated temperature*

The X-ray spectra of the NiAl–W powders after annealing at different temperatures (Fig. 10) show a gradual sharpening of the NiAl and W peaks. Annealing at 600 °C is already sufficient to alter the peak width significantly compared with the mechanically alloyed powders (Fig. 3), indicating that coarsening of the phases or grains, and reduction of the density of defects are taking place. Even after annealing at 1000 °C, the width of the refractory peaks (Fig. 19(a)) is much larger than for bulk refractory metal samples, indicating that the refractory dispersion is still very fine. As shown in part 2 of this paper [37] by electron microscopy, the dispersoid size after hot isostatic pressing at 1000 °C is indeed less than 100 nm.

Thermogravimetry curves (Fig. 11) show that the refractory-containing powders oxidise rapidly above about 425 °C, while the unalloyed NiAl powders exhibit little mass gain up to about 700 °C. Assuming that only alumina forms in the unalloyed NiAl powders, as observed for Al-to-Ni ratios above 0.5 in nickel–aluminum bulk alloys [43], simple mass balance calculations indicate that 27 wt.% of the aluminum present in the powder has been oxidized at 1000 °C; this unusually large mass increase is due to the high area-to-volume ratio of the mechanically alloyed powders. Assuming that the NiAl matrix is oxidizing at the same rate in the refractory-containing samples as in the unalloyed NiAl sample, and assuming the formation of WO_3 and MoO_3 respectively, mass calculations predict that 99–134 wt.% of the refractory metal initially present is oxidized at 1000 °C, indicating complete oxidation of the refrac-

tory phase. The values above 100% may be due to a change in the NiAl oxidation mode in the presence of the refractory metal, for example the formation of nickel oxide, or formation of mixed oxides. For the molybdenum-containing samples, rapid acceleration of the oxidation kinetics occurs near 795 °C, corresponding to the melting point of MoO_3 [42,44]. At lower temperatures, a decrease in oxidation kinetics is observed near 650 °C, probably as a result of the oxidation of NiAl which forms a protective oxide layer; a similar but weaker effect is observed for the tungsten-containing powders.

5. Conclusions

Room-temperature synthesis of NiAl in the presence of 10 or 30 vol.% molybdenum or tungsten was performed by reactive mechanical alloying of elemental powders, resulting in a fine dispersion of refractory metal particles in an NiAl matrix. No measurable intermediate intermetallics were observed during synthesis.

Synthesis of the intermetallic NiMo was achieved by hydrogen reduction at 1000 °C of finely dispersed nickel oxide and molybdenum oxide in stoichiometric proportions. Synthesis of NiW by the same technique was only partially successful.

Reactive mechanical alloying of NiMo with metallic nickel and aluminum powders resulted in NiAl containing a fine dispersion of molybdenum, without significant acceleration of the synthesis step, as compared with the direct synthesis route described above. The shape and size of the molybdenum dispersion is affected however; particles are smaller and more equiaxed when the brittle NiMo precursor is used.

The synthesized powders were stable on heat treatment for 1 h at 1000 °C in a reducing atmosphere, as expected from the fact that NiAl forms a simple eutectic with both molybdenum and tungsten at 1600 °C.

Rapid mass-gain of all mechanically alloyed powders resulted from heating in air above about 425 °C, as a result of oxidation of the refractory phase and the matrix. Owing to the small size of the powders, the NiAl matrix did not provide effective protection from oxidation.

Acknowledgments

T.T. acknowledges a fellowship from Honny Chemical Corp. and D.C.D. is grateful for the support of AMAX, in the form of an endowed chair at MIT.

References

[1] J.D. Cotton and M.J. Kaufman, *Scr. Metall. Mater., 25* (1991) 1827.
[2] P. Nash, in C.C. Koch, C.T. Liu and N.S. Stoloff (eds.), *High-Temperature Ordered Intermetallic Alloys*, MRS, Pittsburgh, PA, 1984, p. 423.
[3] F.H. Hayes, P. Rogl and E. Schmidt, in G. Petzow and G. Effenberg (eds.), *Ternary Alloys*, Vol. 8, VCH, New York, 1993, p. 40.
[4] M.R. Jackson and J.L. Walter, in B.H. Kear, D.R. Muzyka, J.K. Tien and S.T. Wlodek (eds.), *Superalloys: Metallurgy and Manufacture*, Claitor, Baton Rouge, LA, 1976, p. 341.
[5] J.L. Walter and H.E. Cline, *Metall. Trans., 1* (1970) 1221.
[6] P. Rogl, in G. Petzow and G. Effenberg (eds.), *Ternary Alloys*, Vol. 4, VCH, New York, 1991, p. 400.
[7] S.B. Maslenkov and V.A. Rodimkina, *Izv. Akad. Nauk SSSR Metally, 3* (1986) 218.
[8] D.R. Johnson, S.M. Joslin, B.F. Oliver, R.D. Noebe and J.D. Whittenberger, in D.B. Miracle, D.L. Anton and J.A. Graves (eds.), *Intermetallic Matrix Composites II*, MRS, Pittsburgh, PA, 1992, p. 87.
[9] H.E. Cline, J.L. Walter, E. Lifshin and R.R. Russell, *Metall. Trans., 2* (1971) 189.
[10] O. Kubaschewski, in G. Petzow and G. Effenberg (eds.), *Ternary Alloys*, Vol. 7, VCH, New York, 1993, p. 199.
[11] Z.M. Alekseeva, in G. Petzow and G. Effenberg (eds.), *Ternary Alloys*, Vol. 8, VCH, New York, 1993, p. 49.
[12] J.G. Webber and D.C. Van Aken, *Scr. Metall. Mater., 23* (1989) 193.
[13] D.P. Mason, D.C. Van Aken, R.D. Noebe, I.E. Locci and K.L. King, in L.A. Johnson, D.P. Pope and J.O. Stiegler (eds.), *High-Temperature Ordered Intermetallic Alloys IV*, MRS, Pittsburgh, PA, 1990, p. 1033.
[14] D.C. Van Aken, D.P. Mason, S.G. Malhotra and J.G. Webber, *J. Mater. Res., 8* (1993) 2524.
[15] M. McLean, *Directionally Solidified Materials for High Temperature Service*, The Metals Society, London, 1983.
[16] D.R. Johnson, S.M. Joslin, R.D. Reviere, B.F. Oliver and R.D. Noebe, in V.A. Ravi and T.S. Srivatsan (eds.), *Processing and Fabrication of Advanced Materials for High Temperature Applications II*, TMS, Warrendale, PA, 1992, p. 77.
[17] K. Vedula, V. Pathare, I. Aslanadis and R.H. Titran, in C.C. Koch, C.T. Liu and N.S. Stoloff (eds.), *High-Temperature Ordered Intermetallic Alloys*, MRS, Pittsburgh, PA, 1984, p. 411.
[18] J.W. Hutchinson and R.M. McMeeking, in S. Suresh, A. Mortensen and A. Needleman (eds.), *Fundamentals of Metal Matrix Composites*, Butterworth-Heinemann, Boston, MA, p. 158.
[19] P.S. Gilman and J.S. Benjamin, *Annu. Rev. Mater. Sci., 13* (1983) 279.
[20] C.C. Koch, *Annu. Rev. Mater. Sci., 19* (1989) 121.
[21] E. Ivanov, T. Grigorieva, G. Golubkova, V. Boldyrev, A.B. Fasman, S.D. Mikhailenko and O.T. Kalinina, *Mater. Lett., 7* (1988) 51.
[22] G. Cocco, S. Enzo, L. Schiffini and L. Battezzati, in E. Arzt and L. Schultz (eds.), *New Materials by Mechanical Alloying Techniques*, DGM Oberursel, Germany, 1990, p. 343.
[23] T. Itsukaichi, S. Shiga, K. Masuyama, M. Umemoto and I. Okane, *Mater. Sci. Forum, 88–90* (1992) 631.
[24] P.A. Vityaz, A.A. Kolesnikov, A.S. Stephanovich and V.F. Nozdrin, *Mater. Sci. Forum, 88–90* (1992) 619.
[25] H. Schröpf, C. Kuhrt, E. Arzt and L. Schultz, *Scr. Metall. Mater., 30* (1994) 1569.

[26] T.R. Bieler, R.D. Noebe, J.D. Whittenberger and M.J. Luton, in D.B. Miracle, D.L. Anton and J.A. Graves (eds.), *Intermetallic Matrix Composites II*, MRS, Pittsburgh, PA, 1992, p. 165.
[27] J.D. Whittenberger, E. Arzt and M.J. Luton, in D.L. Anton, P.L. Martin, D.B. Miracle and R. McMeeking (eds.), *Intermetallic Matrix Composites*, MRS, Pittsburgh, PA, 1990, p. 211.
[28] B. Huang, J. Vallone, C.F. Klein and M.J. Luton, in D.B. Miracle, D.L. Anton and J.A. Graves (eds.), *Intermetallic Matrix Composites II*, MRS, Pittsburgh, PA, 1992, p. 171.
[29] J.D. Whittenberger, E. Arzt and M.J. Luton, *J. Mater. Res., 194* (1990) 271.
[30] S.J. Hwang, P. Nash, M. Dollar and S. Dymek, in L.A. Johnson, D.P. Pope and J.O. Stiegler (eds.), *High-Temperature Ordered Intermetallic Alloys IV*, MRS, Pittsburgh, PA, 1990, p. 661.
[31] S. Dymek, M. Dollar, S.J. Hwang and P. Nash, *Mater, Sci. Eng., A152* (1992) 160.
[32] S. Dymek, S.J. Hwang, M. Dollar, J.S. Kallend and P. Nash, *Scr. Metall. Mater., 27* (1992) 161.
[33] E. Arzt, E. Gohring and P. Grahle, in I. Baker, R. Darolia, J.D. Whittenberger and M.H. Yoo (eds.), *High-Temperature Ordered Intermetallic Alloys V*, MRS, Pittsburgh, PA, 1993, p. 861.
[34] S.J. Hwang, P. Nash, M. Dollar and S. Dymek, *Mater. Sci. Forum, 88–90* (1992) 611.
[35] T. Takahashi and D.C. Dunand, *Mater. Sci. Eng., 192/193* (1995) 195–203.
[36] A.J. Hickl and R.W. Heckel, *Metall. Trans. A, 6* (1975) 431.
[37] D.C. Dunand, *J. Mater. Sci., 29* (1994) 4056.
[38] K.S. Hwang and Y.C. Lu, in E.R. Andreotti and P.J. McGeehan (eds.), *1990 Advances in Powder Metallurgy*, Metal Powder Industries Federation, Princeton, NJ, 1990, p. 133.
[39] S.C. Ur and P. Nash, *Metall. Mater. Trans. A, 25* (1994) 871.
[40] C. Kuhrt, H. Schroepf, L. Schultz and E. Arzt, in J.J. deBarbadillo, F.H. Froes, R. Schwarz (eds.), *Second Int. Conf. on Structural Applications of Mechanical Alloying*, ASM, Materials Park, OH, 1993, p. 269.
[41] *Metals Handbook: Alloy Phase Diagrams*, American Society for Metals, Metals Park, OH, 1992.
[42] T.B. Reed, *Free Energy of Formation of Binary Compounds: An Atlas of Charts for High-Temperature Chemical Calculations*, MIT Press, Cambridge, MA, 1971.
[43] J.L. Smialek and G.H. Meier, in C.T. Sims, N.S. Stoloff and W.T. Hagel (eds.), *Superalloys II*, Wiley, New York, 1987, p. 293.
[44] R.C. Weast (ed.), *Handbook of Chemistry and Physics*, CRC Press, Boca Raton, FL, 1988.